

Nonconservative Coupling in a Passive Silicon Microring Resonator

H. Du^{1,*}, X. Zhang,² C. G. Littlejohns,^{1,3} D. T. Tran,¹ X. Yan,¹ M. Banakar,¹ C. Wei^{1,3}, D. J. Thomson,¹ and G. T. Reed¹

¹Optoelectronics Research Centre, University of Southampton, Southampton SO17 1BJ, United Kingdom

²Department of Electrical Engineering, Pennsylvania State University, University Park, Pennsylvania 16802, USA

³Silicon Technologies Centre of Excellence, Nanyang Technological University, 639798 Singapore



(Received 25 July 2019; published 9 January 2020)

The authors report on nonconservative coupling in a passive silicon microring between its clockwise and counterclockwise resonance modes. The coupling coefficient is adjustable using a thermo-optic phase shifter. The resulting resonance of the supermodes due to nonconservative coupling is predicted in theory and demonstrated in experiments. This Letter paves the way for fundamental studies of on-chip lasers and quantum photonics, and their potential applications.

DOI: [10.1103/PhysRevLett.124.013606](https://doi.org/10.1103/PhysRevLett.124.013606)

The coupling between resonant modes in optical resonators on a silicon photonics platform is the cornerstone for many fundamental physics systems and practical applications [1–7]. In particular, the tuning of coupling strength between two resonant modes is critical to entanglement generation in photonics [8,9], improvement of single photon statistics [10], spontaneous symmetry breaking [11], and more, where precise values of coupling strength are required to achieve corresponding phenomena. Even though optical resonators are inherently dissipative, most previous studies focus on the tailoring of coupling strength within the domain of conservative coupling, which assumes that the losses of the systems are essentially negligible. However, the nondissipative assumption is a valid approximation only in extremely ultrahigh quality factor (Q factor) systems, where the photon lifetime is long enough that the energy dissipation is negligible. Strictly speaking, the mode coupling in optical resonators is actually nonconservative coupling, in which the coupling coefficient is a complex number, described by a coupling amplitude and a coupling phase. Therefore, it is of great significance to study the nonconservative mode coupling, which can not only rigorously describe the mode coupling in optical resonators but also enable functional resonant photonic devices. For example, in a coupled-cavity semiconductor laser, the complex coupling coefficient, involving absolute coupling strength and relative phase, has a crucial effect on its single mode operation, phase locking, and mode stability [12,13]. In addition, nonconservative coupling can be used to induce parity-time symmetry (PT symmetry) breaking in coupled resonators [14]. The study of nonconservative coupling can also be applied to topological optics for light steering [15].

In this Letter, for the first time, we report on the tunable nonconservative coupling in a passive silicon microring resonator between its clockwise (CW) and counterclockwise (CCW) traveling resonant modes. “Passive” used in this Letter is to describe photonic devices which do not

generate, amplify, modulate, or detect light but can guide it with low or negligible losses. Frequency split is widely observed in microring resonators [16,17], due to the backscattering effect of the ring sidewall roughness, also known as degeneracy lifting [18]. In our study, to enable tunable nonconservative intermode coupling, an integrated thermal phase shifter and a Sagnac loop mirror are utilized to adjust the complex coupling coefficient between the clockwise and counterclockwise resonant modes through thermal-optic effects. Consequently, various frequency and/or loss splitting phenomena are observed in the microring resonator.

We first employ coupled mode theory to describe the nonconservative coupling effect in a ring resonator configured as an add-drop filter. The coupled mode equations can be given by

$$\frac{d}{dt}a = \left(i\omega_a - \frac{1}{\tau_{ia}} - \frac{2}{\tau_{ea}} \right) a - i\mu_{ba}b, \quad (1)$$

$$\frac{d}{dt}b = \left(i\omega_b - \frac{1}{\tau_{ib}} - \frac{2}{\tau_{eb}} \right) b - i\mu_{ab}a, \quad (2)$$

where a and b denote the amplitude of the CW and CCW modes, respectively; $\omega_{a,b}1/\tau_{ia,ib}$ and $1/\tau_{ea,eb}$ denote their natural resonance frequency, intrinsic loss, and the loss due to the coupling between the ring and waveguide, respectively. μ_{ba} and μ_{ab} denote the coupling coefficient from mode b to a and from a to b , respectively. Here, the coupling coefficient is defined as $\mu_{ab,ba} = \omega \int (\epsilon - \epsilon_0) \mathbf{e}_{a,b}^* \mathbf{e}_{b,a} dV$ [19]. Also, ϵ and ϵ_0 are the permittivities of the photonic material and its surroundings; \mathbf{e}_i and \mathbf{e}_j denote the electrical field profiles of the two modes. For the conservative coupling, we can have $(d/dt)(|a|^2 + |b|^2) = 0$, and thus $\mu_{ba} = \mu_{ab}^* = \mu_0$. Therefore, $\mu_{ab,ba}$ is real for the conservative coupling situation. Besides, owing to the optical reciprocity, the

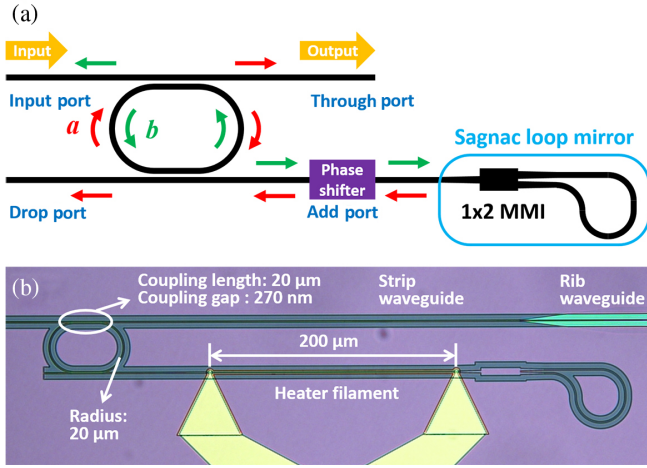


FIG. 1. (a) Schematic of the nonconservative coupling mechanism investigated in this Letter. (b) Optical image of the device tested.

inherent nature of the two modes must be the same, that is, $\omega_a = \omega_b = \omega_0$, $\tau_{ia} = \tau_{ib}$, and $\tau_{ea} = \tau_{eb}$.

However, in the device designed for this Letter as schematized in Fig. 1(a), a Sagnac loop mirror is installed at the add port, making μ_{ba} different. The modified coupled mode equations to describe the new situation can be given as below:

$$\frac{d}{dt}a = \left(i\omega_0 - \frac{1}{\tau_i} - \frac{2}{\tau_e} \right) a - i \left(\mu_0 + r \frac{1}{\tau_e^2} e^{i\varphi} \right) b, \quad (3)$$

$$\frac{d}{dt}b = \left(i\omega_0 - \frac{1}{\tau_i} - \frac{2}{\tau_e} \right) b - i\mu_0 a. \quad (4)$$

Here, μ_0 denotes the mutual coupling coefficient due to the sidewall roughness, and $r(1/\tau_e^2)e^{i\varphi}$ denotes the coupling from mode b to mode a due to the mirror. r is a real constant describing the reflection coefficient, which is determined by the reflection ratio from the Sagnac loop

mirror and the propagation loss between the ring and the mirror. φ denotes the relative phase, which can be tuned using the thermo-optic phase shifter integrated between the ring and the mirror.

In this situation, $\mu_{ba} = \mu_0 + r(1/\tau_e^2)e^{i\varphi}$ is a complex number and $\mu_{ba} \neq \mu_{ab}^*$, indicating nonconservative coupling. The eigenvalue of the modified equations can be solved as

$$\chi_{1,2} = \omega_0 + i \frac{1}{\tau_i} \pm \sqrt{\mu_0 [\mu_0 + r(1/\tau_e^2)e^{i\varphi}]}, \quad (5)$$

where $(1/\tau_i) = (1/\tau_i) + (2/\tau_e)$, denoting the total loss. The real part of the eigenvalue $[\text{Re}(\chi_{1,2})]$ denotes the resonance frequency of the supermode, while the imaginary part $[\text{Im}(\chi_{1,2})]$ denotes its loss. As can be seen in Eq. (5), with different complex coupling coefficients, the complex eigenvalues are also different, leading to frequency split ($2\text{Re}\{\sqrt{\mu_0[\mu_0 + r(1/\tau_e^2)e^{i\varphi}]}\}$) and/or loss split ($2\text{Im}\{\sqrt{\mu_0[\mu_0 + r(1/\tau_e^2)e^{i\varphi}]}\}$). All of the mode splitting cases can be predicted from Eq. (5), and they are summarized in Table I. It is interesting to see that both frequency split and loss split can be realized, while only frequency split can be obtained in conservative coupling situations if the two coupled resonators are identical [16,17,20,21].

To demonstrate our theoretical prediction in Table I, a device is fabricated on 220 nm SOI platform using the CORNERSTONE rapid prototyping service [22] as shown in Fig. 1(b), in which some of the key device dimensions are annotated. The device is based on strip waveguides with a width of 385 nm, making the light very sensitive to sidewall roughness and thus making mode split stronger. The phase shifter is made of a TiN filament working with the thermo-optic effect, using which the relative phase φ can be manipulated.

In experiments, the spectrum of the device is measured at an initial situation as the lavender curve in Fig. 2. Several peaks are detected which denote the different resonant conditions of the ring resonator associated with

Table I. Summary of resonance split cases for nonconservative coupling with different conditions.

		Frequency split [$\text{Re}(\chi_1) \neq \text{Re}(\chi_2)$]	Loss split [$\text{Im}(\chi_1) \neq \text{Im}(\chi_2)$]	Comments
Case 1	$q \approx 0, p > 0$	Yes	No	Typical phenomenon in conservative coupling
Case 2	$q \neq 0, p \approx 0$	No	Yes	Typical phenomenon in dissipative coupling
Case 3	$q \approx 0, p \approx 0$	No	No	$\chi_1 \approx \chi_2$
Case 4	$q > 0, p > 0$	Yes	Yes	Resonance with smaller resonance wavelength has higher loss
Case 5	$q < 0, p > 0$	Yes	Yes	Resonance with smaller resonance wavelength has lower loss

Note that $\sqrt{\mu_0[\mu_0 + r(1/\tau_e^2)e^{i\varphi}]} = iq + p$. p and q , respectively, denote the changes in the real and imaginary parts of the eigenvalue induced by the thermal phase shifter.

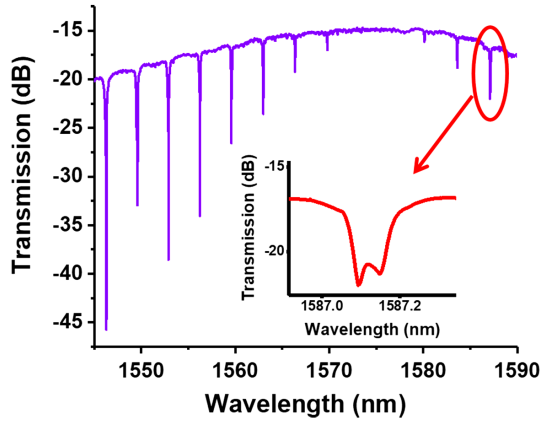


FIG. 2. Spectrum of the device in the initial situation without thermal tuning.

the constructive interference at different wavelengths. A resonant condition is selected for this Letter and plotted in detail in the inset of Fig. 2. As can be seen, this resonance has a frequency split at the initial situation. [The selected mode is chosen because it can cover most cases listed in Table I. As can be seen, the resonance mode selected has a relatively lower extinction ratio (coupling depth), in which case there is relatively more optical power coupled to the add port. Thus, more power is reflected and coupled back to the ring resonator.] We then replot the selected resonance spectrum in linear scale and fit the splitting resonance with a two-peak Lorentz fitting [see Fig. 3(a)], through which we can determine the complex eigenvalues of the resonance supermodes [Eq. (5)]. As can be seen in Fig. 3(a), both frequency and loss splitting are observed, and the resonance with shorter wavelength has lower loss, which corresponds to case 5 in Table I. Note that the split (or nonsplit) modes are

superposition modes formed by the CW and CCW modes. Any individual spectrum dip of a split resonance does not correspond to a CW or CCW mode.

When electrical power is applied to the thermo-optic phase shifter, the relative phase φ is manipulated, which can further tune the complex coupling coefficient. The spectra at different thermal phase shifter powers are plotted on a linear scale in Figs. 3(a)–3(f), in which the dashed orange curves indicate the measured spectra, and the blue solid curves denote the two-peak Lorentz fitting results, while the green and red curves are the individual Lorentz spectra to form the double peak resonance. From these individual Lorentz fittings, the Q factors of the individual resonances can be obtained, which are annotated in the subfigures. The real and imaginary parts of the eigenvalues obtained from the fitted spectra are listed in Table II. [Note that $\text{Im}(\chi_{1,2}) = 4\pi\omega_0/Q$.]

Specifically, when a thermal phase shifter power of 1.4 mW is applied [Fig. 3(b)], the loss split increases, and it is typically case 5 (Table II). By increasing the thermal phase shifter power to 5.6 mW [Fig. 3(c)], almost no frequency split can be observed, but loss split is observed, indicating case 2. If the thermal phase shifter power is further increased to 12.6 mW [Fig. 3(d)], typically case 4 can be realized, in which there is both frequency split and loss split but where the resonance with shorter wavelength has higher loss. When the thermal phase shifter power reaches 14.3 mW [Fig. 3(e)], the split two resonances have almost the same loss, indicating case 1. After that, when the thermal phase shifter power is increased to 15.3 mW, the resonance case goes back to case 5, similar to the initial situation [Fig. 3(f)]. In Table II, the applied heating powers are converted into phase shift values using the method discussed in Sec. I of the Supplemental Material [23]. As can be seen, the resonance goes back to a similar case

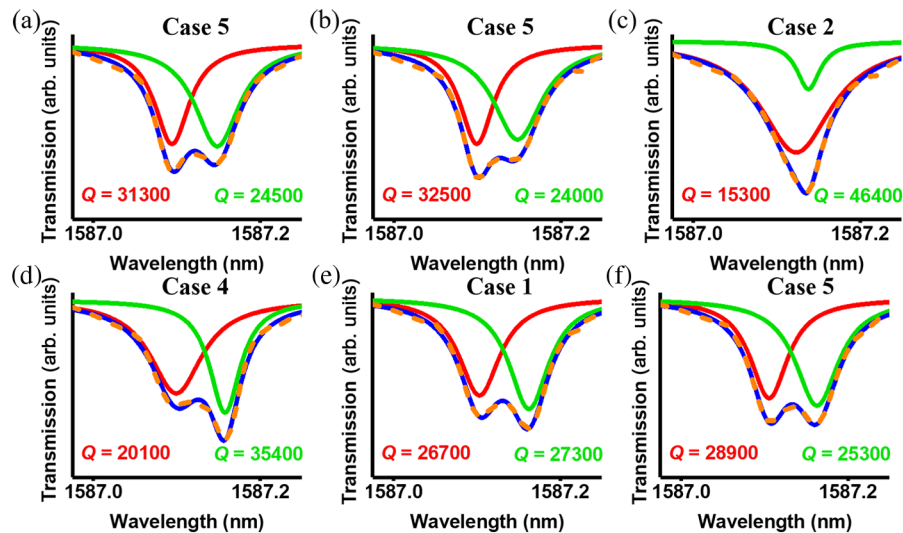


FIG. 3. Resonance tuning results with respect to different thermal phase shifter powers [(a) 0, (b) 1.4, (c) 5.6, (d) 12.6, (e) 14.3, and (f) 15.3 mW]. All of the spectra are plotted on a linear scale.

Table II. Eigenvalue results of the supermodes resulting from nonconservative coupling.

Applied power (mW)	Phase shift	Case no.	Eigenvalue, $\chi_{1,2} \approx$ (THz)	Sign of p and q	
				p	q
0	0	5	$(188.8955 \pm 0.003225) * 2\pi - i(0.0431 \pm 0.0053)$	>0	<0
1.4	$0.09 * 2\pi$	5	$(188.8952 \pm 0.002905) * 2\pi - i(0.0446 \pm 0.0081)$	>0	<0
5.6	$0.36 * 2\pi$	2	$(188.8943 \pm 0.000875) * 2\pi + i(0.0516 \pm 0.0260)$	≈ 0	>0
12.6	$0.81 * 2\pi$	4	$(188.8946 \pm 0.003480) * 2\pi + i(0.0450 \pm 0.0115)$	>0	>0
14.3	$0.92 * 2\pi$	1	$(188.8941 \pm 0.003535) * 2\pi + i(0.0439 \pm 0.0005)$	>0	≈ 0
15.3	$0.99 * 2\pi$	5	$(188.8939 \pm 0.003420) * 2\pi - i(0.0440 \pm 0.0029)$	>0	<0

with the initial situation after a $\sim 2\pi$ phase shift. Also, the p and q values can be obtained from the eigenvalue results. Their signs are summarized in the last two columns of Table II, which matches the prediction in Table I.

On the other hand, as can be seen in Table II, the central eigenvalue is independent to the applied thermal phase shifter power [i.e., relative phase (φ) shift], while the eigenvalue split width is dependent on the applied thermal phase shifter power [i.e., relative phase (φ) shift], which agrees well with Eq. (5). However, the two split resonance frequencies are too close at the thermal phase shifter power of 5.6 mW, making the two-peak fitting less accurate, which makes the central eigenvalue slightly different from the others.

The nonconservative coupling induced resonance split not only can be tuned by the phase shift of the additional coupling coefficient [i.e., $\text{Arg}[r(1/\tau_c^2)e^{i\varphi}]$] but can also be modified by the amplitude of the additional coupling coefficient [i.e., $\text{Abs}[r(1/\tau_c^2)e^{i\varphi}]$]. If $\text{Abs}[r(1/\tau_c^2)e^{i\varphi}] < \mu_0$, two scenarios of case 1 are achievable with different frequency splits, while case 2 or 3 cannot be obtained. If $\text{Abs}[r(1/\tau_c^2)e^{i\varphi}] \approx \mu_0$, case 1 with only one frequency split scenario can be realized, and case 3 can be obtained, while case 2 is not achievable. If $\text{Abs}[r(1/\tau_c^2)e^{i\varphi}] > \mu_0$, case 1 with only one frequency split scenario can be realized and case 2 can be obtained, while case 3 is not achievable. These analyses are summarized in Table III, with discussion on cases 4 and 5 included. In this Letter, the thermal phase shifter can vary only the relative phase of the reflection from the Sagnac loop mirror, that is, $\text{Abs}[r(1/\tau_c^2)e^{i\varphi}]$ is inherent and constant, while $\text{Arg}[r(1/\tau_c^2)e^{i\varphi}]$ is tunable. If we compare Table III with Table II, we can see that all five cases have been realized

in our experiment except for case 3, indicating that $\text{Abs}[r(1/\tau_c^2)e^{i\varphi}] > \mu_0$ in our experiment (also see Sec. II of the Supplemental Material [23]).

In summary, we have theoretically and experimentally demonstrated nonconservative coupling in a passive silicon microring resonator with tunability between the CW and CCW resonance modes. The mechanism is based on add-drop filter configuration with a mirror boundary at the add port, and a phase shifter is added between the ring resonator and the mirror to make the coupling tunable. The resonances under different situations—that is, different relative phases of the reflection—are theoretically predicted using coupled mode theory. In experiments, a prototype is tested, and predicted results are validated. With the proposed nonconservative coupling, resonances with or without frequency split and with or without loss split can be realized on the resulting supermodes. With the phase shifter, the resonance cases can also be switched by applying different thermal phase shifter powers. In addition, our tuning method for the nonconservative coupling has potential applications in coupled-cavity lasers for mode selectivity which relies on coupling phase (in phase coupling or $\pi/2$ phase coupling) [12]. Thus, we believe that the nonconservative coupling investigated in this Letter has promising potential in on-chip lasers for future integrated photonic systems. Aside from this, under certain conditions [i.e., $\text{Abs}[r(1/\tau_c^2)e^{i\varphi}] \approx \mu_0$ in Table III], it is possible to realize exceptional points where the eigenvalues of the ring resonator coincide [i.e., $\text{Im}(\chi_1) = \text{Im}(\chi_2)$, $\text{Re}(\chi_1) = \text{Re}(\chi_2)$] [24,25]. See Sec. II of the Supplemental Material for details [23]. This may potentially benefit exceptional points enhanced sensing with our fine-tuning method [26,27]. However, owing to the limit

Table III. Summary of the viability of the resonance cases with different conditions.

	$\text{Abs}[r(1/\tau_c^2)e^{i\varphi}] < \mu_0$	$\text{Abs}[r(1/\tau_c^2)e^{i\varphi}] \approx \mu_0$	$\text{Abs}[r(1/\tau_c^2)e^{i\varphi}] > \mu_0$
Case 1	Achievable with different frequency split.	Achievable with one frequency split.	Achievable with one frequency split.
Case 2	Not achievable.	Not achievable.	Achievable.
Case 3	Not achievable.	Achievable.	Not achievable.
Case 4	Achievable. The loss splitting value is limited by $\text{Abs}[(1/\tau_c^2)e^{i\varphi}]$.		
Case 5	Achievable. The loss splitting value is limited by $\text{Abs}[(1/\tau_c^2)e^{i\varphi}]$.		

of our current condition [i.e., $\text{Abs}[r(1/\tau_e^2)e^{i\varphi}] > \mu_0$ in Table III], we cannot fulfill the exceptional points conditions. Nevertheless, we can reach the broken- PT -symmetric region [where $\text{Im}(\chi_1) \neq \text{Im}(\chi_2)$, $\text{Re}(\chi_1) \approx \text{Re}(\chi_2)$] by tuning the phase shift without attendant exceptional points [28], which may find applications in passive reciprocity breaking [29]. On the other hand, the demonstrated nonconservative coupling indicates the non-Hermiticity of our system. Traditional non-Hermitian systems are designed utilizing gain-loss contrast and the PT symmetry breaking is based on “gain-saturation nonlinearity” [24]. However, the nonconservative coupling mechanism discussed in this Letter demonstrates non-Hermiticity without gain. Loss split is theoretically predicted and experimentally observed in our work (see Sec. II of the Supplemental Material for details [23]). If we see the two resonance modes with different losses as lossless mode and lossy mode separately, similar PT symmetry breaking can also be achieved based on “loss-induced optical transparency” [30,31]. Thus, nonreciprocity can be realized in our tunable non-Hermitian system without gain as long as loss nonlinearity can build up [24]. In addition, this achievement can be applied to light steering. For example, by employing our tunable nonconservative coupling method in a 2D photonic topological microring array, topological light steering [15] can be potentially realized, but the optical pumping and gain materials are not required. Specifically, by tuning nonconservative coupling, we may create topological states at the boundary of the lossless and lossy domain of rings’ array based on the PT symmetry breaking [15,32]. As such, light can be guided at the interface of lossless and lossy region of rings. In addition, the tuning mechanism demonstrated in this Letter can be used for postfabrication adjustment and used to switch the state of broken-unbroken PT symmetry. Finally, although the mathematical model established and demonstrated in this Letter is simple, it provides a method to understand and investigate more complicated nonconservative or non-Hermitian systems. In a word, our Letter opens up opportunities for both fundamental and applied studies of nonconservative coupling in future integrated photonic systems and quantum photonics.

All data supporting this study are available upon request from the University of Southampton repository [33].

The authors would like to acknowledge the Engineering and Physical Sciences Research Council (EPSRC) funded CORNERSTONE [22] project (No. EP/L021129/1), through which the prototype device is fabricated. C. G. L. acknowledges support from the National Research Foundation of Singapore (Grant No. NRF-CRP12-2013-04). D. J. T. acknowledges funding from the Royal Society on his University Research Fellowship.

*H.Du@soton.ac.uk

- [1] S. V. Zhukovsky, D. N. Chigrin, A. V. Lavrinenko, and J. Kroha, *Phys. Rev. Lett.* **99**, 073902 (2007).
- [2] X. Yang, M. Yu, D.-L. Kwong, and C. W. Wong, *Phys. Rev. Lett.* **102**, 173902 (2009).
- [3] Y. Sato, Y. Tanaka, J. Upham, Y. Takahashi, T. Asano, and S. Noda, *Nat. Photonics* **6**, 56 (2012).
- [4] M. Notomi, E. Kuramochi, and T. Tanabe, *Nat. Photonics* **2**, 741 (2008).
- [5] B. Johnson *et al.*, *Nat. Phys.* **6**, 663 (2010).
- [6] M. J. Hartmann, F. G. Brandao, and M. B. Plenio, *Nat. Phys.* **2**, 849 (2006).
- [7] H. Altug, D. Englund, and J. Vučković, *Nat. Phys.* **2**, 484 (2006).
- [8] A. Dousse, J. Suffczyński, A. Beveratos, O. Krebs, A. Lemaître, I. Sagnes, J. Bloch, P. Voisin, and P. Senellart, *Nature (London)* **466**, 217 (2010).
- [9] H. Wang *et al.*, *Phys. Rev. Lett.* **106**, 060401 (2011).
- [10] T. C. H. Liew and V. Savona, *Phys. Rev. Lett.* **104**, 183601 (2010).
- [11] P. Hamel, S. Haddadi, F. Raineri, P. Monnier, G. Beaudoin, I. Sagnes, A. Levenson, and A. M. Yacomotti, *Nat. Photonics* **9**, 311 (2015).
- [12] G. P. Agrawal and N. K. Dutta, *Semiconductor Lasers* (Springer Science+Business Media, New York, 2013).
- [13] E. Lafalce, Q. Zeng, C. H. Lin, M. J. Smith, S. T. Malak, J. Jung, Y. J. Yoon, Z. Lin, V. V. Tsukruk, and Z. V. Vardeny, *Nat. Commun.* **10**, 561 (2019).
- [14] B. Peng, Ş. K. Özdemir, F. Lei, F. Monifi, M. Gianfreda, G. L. Long, S. Fan, F. Nori, C. M. Bender, and L. Yang, *Nat. Phys.* **10**, 394 (2014).
- [15] H. Zhao, X. Qiao, T. Wu, B. Midya, S. Longhi, and L. Feng, *Science* **365**, 1163 (2019).
- [16] Z. Zhang, M. Dainese, L. Wosinski, and M. Qiu, *Opt. Express* **16**, 4621 (2008).
- [17] Q. Li, Z. Zhang, F. Liu, M. Qiu, and Y. Su, *Appl. Phys. Lett.* **93**, 081113 (2008).
- [18] P.-Y. Bourgeois and V. Giordano, *IEEE Trans. Microwave Theory Tech.* **53**, 3185 (2005).
- [19] H. A. Haus and W. Huang, *Proc. IEEE* **79**, 1505 (1991).
- [20] A. Li and W. Bogaerts, *Photonics Res.* **6**, 620 (2018).
- [21] A. Li, T. Van Vaerenbergh, P. De Heyn, P. Bienstman, and W. Bogaerts, *Laser Photonics Rev.* **10**, 420 (2016).
- [22] <http://www.cornerstone.sotonfab.co.uk/>.
- [23] See Supplemental Material at <http://link.aps.org/supplemental/10.1103/PhysRevLett.124.013606> for more experimental data and theoretical analysis to support this Letter.
- [24] Ş. Özdemir, S. Rotter, F. Nori, and L. Yang, *Nat. Mater.* **18**, 783 (2019).
- [25] H. Zhou, J. Y. Lee, S. Liu, and B. Zhen, *Optica* **6**, 190 (2019).
- [26] W. Chen, Ş. K. Özdemir, G. Zhao, J. Wiersig, and L. Yang, *Nature (London)* **548**, 192 (2017).
- [27] H. Hodaei, A. U. Hassan, S. Wittek, H. Garcia-Gracia, R. El-Ganainy, D. N. Christodoulides, and M. Khajavikhan, *Nature (London)* **548**, 187 (2017).
- [28] Y. N. Joglekar and A. K. Harter, *Photonics Res.* **6**, A51 (2018).

- [29] B. Zhen, C. W. Hsu, Y. Igarashi, L. Lu, I. Kaminer, A. Pick, S.-L. Chua, J. D. Joannopoulos, and M. Soljačić, *Nature (London)* **525**, 354 (2015).
- [30] A. Guo, G. J. Salamo, D. Duchesne, R. Morandotti, M. Volatier-Ravat, V. Aimez, G. A. Siviloglou, and D. N. Christodoulides, *Phys. Rev. Lett.* **103**, 093902 (2009).
- [31] N. M. Litchinitser and V. M. Shalaev, *Nat. Photonics* **3**, 75 (2009).
- [32] S. Weimann, M. Kremer, Y. Plotnik, Y. Lumer, S. Nolte, K. G. Makris, M. Segev, M. C. Rechtsman, and A. Szameit, *Nat. Mater.* **16**, 433 (2017).
- [33] See <https://doi.org/10.5258/SOTON/D1003>.